CMS Physics Analysis Summary

Contact: cms-pag-conveners-top@cern.ch 2019/03/16

Measurement of differential cross sections and charge ratios for t-channel single top quark production at 13 TeV

The CMS Collaboration

Abstract

A measurement is presented of differential cross sections for t-channel single top quark production in proton-proton collisions at a centre-of-mass energy of 13 TeV by the CMS experiment at the LHC. Events containing single muons or electrons and two or three jets are analysed, corresponding to an integrated luminosity of 36 fb^{-1}. The cross section is measured as a function of the top quark transverse momentum, rapidity, and polarization angle, the charged lepton transverse momentum and rapidity, and the transverse momentum of the W boson from the top quark decay. In addition, the charge ratio, defined as the ratio of the single top quark cross section to the sum of the single top quark and antiquark cross sections, is measured differentially as a function of the top quark, charged lepton, and W boson kinematic observables. The results are found to be in agreement with predictions using various next-to-leading order event generators and various sets of parton distribution functions. Additionally, the spin asymmetry, sensitive to the top quark polarisation, is determined from the differential distribution of the polarisation angle at parton level to be 0.439 ± 0.062, in agreement with the standard model prediction using the POWHEG event generator at next-to-leading order.

1 Introduction

The three main production modes of single top quarks and antiquarks in proton-proton (pp) collisions via electroweak interactions are commonly categorised through the virtuality of the exchanged W boson. They are called t channel (t ch.) when the W boson is space-like, s channel when it is time-like, and W-associated (tW) when the W boson is on shell. The production via the t channel has the largest cross section of the three at the LHC. Its main Feynman diagrams are presented in Fig. 1. The t-channel cross section in pp collisions at a centre-of-mass energy of 13 TeV is predicted as $\sigma_{\mathrm{t}} = 136.0^{+5.4}_{-4.6}$ pb for the top quark and $\sigma_{\bar{\mathrm{t}}} = 81.0^{+4.1}_{-3.6}$ pb for the top antiquark, respectively, as calculated for a top quark mass of 172.5 GeV at next-to-leading order (NLO) in quantum chromodynamics (QCD) using the Hathor v2.1 [1, 2] program. The parton distribution function (PDF) and α_{S} uncertainties are calculated using the PDF4LHC prescription [3] with the MSTW2008 68% confidence level (CL) NLO [4, 5], CT10 NLO [6], and NNPDF2.3 [7] PDF sets, and are added in quadrature with the renormalisation and factorisation scale uncertainty. These predicted cross sections have been used for normalising the corresponding simulated samples of single top quark and antiquark events employed in this measurement, which were generated with similar settings. Predictions at next-to-next-to-leading order are available as well [8] but are not utilised since those have been calculated using a different PDF set and top quark mass value. In the rest of this note, the word "quark" is used to generically denote a quark or an antiquark, unless specified.

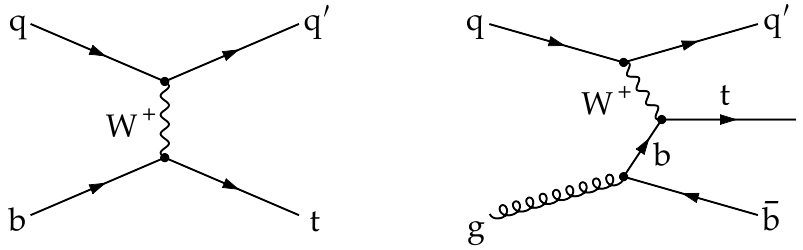

Figure 1: Born-level Feynman diagrams for single top quark production in the t channel: (left) $(2) \to (2)$ and (right) $(2) \to (3)$ processes. Corresponding diagrams exist for single top antiquark production.

The t-channel production mode was first observed at the Tevatron [9, 10] and is since then well established at the LHC [11–16]. Its inclusive cross section has been measured with high precision in pp collisions at centre-of-mass energies of 7, 8, and 13 TeV. Differential cross sections have been measured as well at centre-of-mass energies of 7 and 8 TeV [12, 14, 17]. Differential measurements help to set constraints on effective field theory operators [18] as well as the top quark mass, the choice of the renormalisation and factorisation scales, and the PDFs [2]. In particular, the ratio of the t-channel top quark production to the top antiquark production is sensitive to the ratio of the up quark to the down quark content of the proton [8, 19]. Furthermore, differential angular distributions can be used to assess the electroweak coupling structure at the Wtb vertex. A "vector-axial-vector" (V-A) coupling is predicted in the standard model (SM), leading to the production of highly polarised top quarks [20–22]. A powerful observable to investigate the coupling structure in t-channel production is given by the top quark polarisation angle $\theta^{\star}_{\mathrm{pol.}}$, defined by

$$\cos\theta^{\star}_{\mathrm{pol.}} = \frac{\vec{p}^{\,(\mathrm{top})}_{\mathrm{q}'} \cdot \vec{p}^{\,(\mathrm{top})}_{\ell}}{|\vec{p}^{\,(\mathrm{top})}_{\mathrm{q}'}| \cdot |\vec{p}^{\,(\mathrm{top})}_{\ell}|}\,, \tag{1}$$

where the momenta of the charged lepton, $\ell \in \{e, \mu\}$, and the spectator quark, q', are calculated in the top quark rest frame. The normalised differential cross section as a function of $\cos\theta^{\star}_{\text{pol.}}$ at the parton level is related to the top quark polarisation, P, as

$$\frac{d\sigma}{\sigma \cdot d\cos\theta^{\star}_{\text{pol.}}} = \frac{1}{2}\left(1 + 2A_{\ell}\cos\theta^{\star}_{\text{pol.}}\right), \quad A_{\ell} = \frac{1}{2}P \cdot \alpha_{\ell}, \tag{2}$$

where A_{ℓ} denotes the spin asymmetry and α_{ℓ} the so-called spin-analysing power of the charged lepton from the top quark decay [22]. The spin asymmetry and/or polarisation has been measured in pp collision data by the ATLAS and CMS Collaborations at a centre-of-mass energy of 8 TeV using various analysis techniques [17, 23, 24].

In this note the differential cross section of single top quarks and antiquarks in the t channel, $d\sigma_{t+\bar{t}}$, is measured at the CERN LHC by the CMS experiment at a centre-of-mass energy of 13 TeV as a function of the top quark transverse momentum, rapidity, and polarisation angle, the transverse momentum and rapidity of the charged lepton ℓ (electron or muon) that originates from the top quark decay $t \to bW \to b\ell\nu$, and the transverse momentum of the W boson from the top quark decay. From the measured differential cross section with respect to the polarisation angle, the spin asymmetry is determined. Additionally, a novel measurement of the differential charge ratio $d(\sigma_t/\sigma_{t+\bar{t}})$ is performed as a function of the transverse momenta and rapidities of the top quark and charged lepton, and the transverse momentum of the W boson from the top quark decay. These measurements are performed at both the parton and particle levels, following the conventions presented in Ref. [25].

An outline of the note is as follows. A summary of the analysed data set and the utilised samples of simulated events is given in Section 2. The reconstruction of physics objects and the event selection are detailed in Section 3. A data-driven procedure to estimate the amount of multijet events remaining after the event selection is provided in Section 4. Section 5 describes the measurement of the amount of t-channel single top quark events from data through a maximum-likelihood (ML) fit. The resulting distributions of the unfolding observables are validated in control and signal regions in Section 6 after scaling the predictions to the fit result. The fit results are used to determine the differential cross sections and charge ratios at the parton and particle levels through an unfolding procedure, as detailed in Section 7. The sources of systematic uncertainties considered are described in Section 8. The results are presented in Section 9. A summary can be found in Section 10.

2 Data set and simulated samples

The analysed pp collision data set corresponds to an integrated luminosity of 36 fb^{-1} [26]. Events were triggered by requiring at least one isolated muon candidate with $p_{\text{T}} > 24$ GeV and $|\eta| < 2.4$ or one electron candidate with $p_{\text{T}} > 32$ GeV and $|\eta| < 2.1$, with additional requirements [27] that select genuine electrons with an efficiency of about 80%.

Various samples of simulated events are used in this measurement for evaluating the detector resolution, efficiencies, and acceptance, as well as estimate the contributions from background processes, define observables, and unfold the differential cross sections at the parton and particle levels.

Single top quark events in the t channel are simulated at NLO in the four flavour scheme (FS) with POWHEG v2 [28, 29] interfaced with PYTHIA v8.2 [30] for the parton shower simulation, using the CUETP8M1 [31] tune interfaced with MADSPIN [32] for simulating the top quark

decay. For comparison, alternative NLO t-channel samples have be generated in 4FS and 5FS using MG5_aMC@NLO v5_2.2.2 [33] interfaced with PYTHIA v8.2 respectively.

The POWHEG v2 generator is also used to simulate events from top quark pair production at NLO. Parton showering is simulated with PYTHIA v8.2 using the CUETP8M2T4 tune [34]. The production of single top quark events via the tW channel is simulated at NLO using POWHEG v1 [35] in 5FS interfaced with PYTHIA v8.2 using the tune CUETP8M1 for parton shower simulation. The overlap with top quark pair production is removed by applying the diagram-removal scheme [36]. Samples of W+jets events are generated with MG5_aMC@NLO v5_2.2.2 at NLO and interfaced with PYTHIA v8.2 using the CUETP8M1 tune. The production of leptonically decaying W bosons in association with jets is simulated with up to two additional partons at matrix element level, and the FxFx scheme [37] is used for merging. Lastly, Z/γ^*+jets events are generated with MG5_aMC@NLO v5_2.2.2 at leading order (LO), interfaced with PYTHIA v8.2 using the MLM matching scheme [38].

In these simulated samples, the NNPDF3.0 [39] set is used as the default PDF and a nominal top quark mass of 172.5 GeV is chosen where applicable.

The simulated events are overlaid with additional collision interactions ("pileup") according to the distribution inferred from the data. All generated events undergo a full GEANT4 [40] simulation of the detector response.

Additional background can come from events containing only jets produced through the strong interaction, which are referred to as "multijet" events in this note. Since the probability for a simulated multijet event to mimic the final state of the signal process is very small, it becomes impractical to simulate a sufficiently large number of events for this background. Therefore, multijet events are modelled using a multijet-event-enriched sideband region from data instead. The method used to model the template and estimate the yield of multijet events in data passing the event selection is detailed in Sections 4 and 5.

3 Event selection

Proton-proton collision events containing one isolated muon or electron and two or three jets are analysed. This signature targets cases where the W boson from a single top quark decays into a charged lepton and a neutrino. One of the selected jets is expected to stem from the hadronisation of a b quark that originates from the top quark decay. Another jet (j') of light flavour (u, d, or s) is expected from the spectator quark (labelled q′ in Fig. 1) that is produced in association with the top quark. Since the spectator quark recoils against the W boson, this jet is characteristically found at relatively low angles with respect to the beam axis.

The particle-flow (PF) algorithm [41] reconstructs and identifies each individual particle in an event with an optimised combination of information from the various elements of the CMS detector [42]. The missing transverse momentum vector, $\vec{p}_{\mathrm{T}}^{\,\mathrm{miss}}$, is defined as the projection onto the plane perpendicular to the beams of the negative vector sum of the momenta of all reconstructed particles in an event. Its magnitude is referred to as missing transverse momentum $p_{\mathrm{T}}^{\mathrm{miss}}$.

Muon candidates are accepted if they have $p_{\mathrm{T}} > 26$ GeV, $|\eta| < 2.4$, and pass the following identification requirements optimised for the selection of prompt muons. A global muon track must have a track fit with a χ^2 per degree of freedom < 10, have hits in the silicon tracker and muon systems, including at least six from the tracker of which at least one must be in the pixel detector. Additionally, muon track segments are required in at least two muon stations,

which suppresses an accidental association of tracks to uncontained hadronic showers spilling into the muon system. Muon candidates are required to be isolated with a relative isolation parameter $I^{\mu}_{\text{rel.}} < 6\%$. The relative isolation parameter is defined by the scalar sum, divided by the p_{T} of the muon, of the transverse energies deposited by stable charged hadrons, photons, and neutral hadrons within a cone of radius $\Delta R = \sqrt{(\Delta\eta)^2 + (\Delta\phi)^2} < 0.4$. Here, $\Delta\eta$ and $\Delta\phi$ are the pseudorapidity and azimuthal angle (in radians), respectively, around the muon direction. The isolation parameter is corrected by subtracting the energy deposited by pileup, which is estimated from the amount of charged hadrons within the isolation cone that are associated with pileup vertices.

Electron candidates are required to have $p_{\text{T}} > 35$ GeV, $|\eta| < 1.479$, and fulfill a set of additional quality requirements as follows: the distance between the matched ECAL cluster position and the extrapolated electron track has to be less than 3.08×10^{-3} and 8.16×10^{-2} rad in η and ϕ, respectively; the absolute difference between the inverse of the energy estimated from the ECAL cluster and the inverse of the electron track momentum must be less than 12.9/MeV; the ratio of the HCAL energy to the ECAL energy associated with the electron is required to be less than 4.14%; the lateral extension of the electron shower in the ECAL is restricted to $\sigma_{\eta\eta} = \sqrt{\sum(\eta_i - \bar{\eta})^2 w_i / \sum w_i} < 9.98 \times 10^{-3}$, where the sum is taken over the 5×5 crystals around the highest E_{T} crystal compatible with the electron candidate, η_i is expressed in terms of unit crystals, $\bar{\eta}$ is the energy-weighted average η of the shower, and w_i denotes the weights that depend logarithmically on the contained energy per crystal. Electrons from photon conversions are suppressed by requiring that the corresponding track has no missing hits in the inner layers of the tracker and any electron-positron pair in the event is incompatible with coming from a photon conversion vertex. Electron candidates have to be isolated using the so-called effective-area-corrected relative isolation parameter [43] by requiring $I^{e}_{\text{rel.}} < 5.88\%$. This parameter is defined similar to the muon isolation parameter by summing the charged and neutral energy within a cone of $\Delta R < 0.3$ around the electron candidate. The contribution from pileup is estimated as $A_{\text{eff}} \cdot \rho$ and subtracted from the isolation parameter, where A_{eff} denote a η-dependent area and ρ is the median of the transverse energy density in a $\delta\eta \times \delta\phi$ region calculated using the charged particle tracks associated with the pileup vertices.

Electron candidates with showers in the ECAL endcap ($1.479 < |\eta| < 2.500$) are not used in the measurement because of the significantly higher background from hadrons misidentified as electrons or electrons from decays of heavy-flavour hadrons, the combination of which we term "nonprompt" electrons.

The selected muon and electron candidates have to be compatible with the primary vertex within $2(0.5)$ mm in the transverse plane and $5\,(1)$ mm along the z-axis for muons (electrons) respectively. The reconstructed vertex with the largest value of summed physics-object p^2_{T} is taken to be the primary pp interaction vertex. The physics objects are the jets, clustered using the jet-finding algorithm described in Refs. [44, 45] with the tracks assigned to the vertex as inputs, and the associated missing transverse momentum, taken as the negative vector sum of the $\vec{p}_{\text{T}}$ of those jets.

Events are rejected if additional muon or electron candidates passing looser selection criteria are present. The selection requirements for these additional muons/electrons are as follows: looser identification and isolation criteria, $p_{\text{T}} > 10\,(15)$ GeV for muons (electrons), and $|\eta| < 2.5$.

Jets are reconstructed from particle-flow candidates and clustered with the anti-k_{T} algorithm [44] with a distance parameter of 0.4 using the FastJet package [45]. The influence of pileup is mitigated using the charged hadron subtraction technique [46]. The jet momentum is determined

as the vectorial sum of all particle momenta in the jet. An offset correction is applied to the transverse jet momenta to account for contributions from pileup. Further corrections are applied to account for the nonuniform detector response in η and p_{T} of the jets. The corrected jet momentum is found from simulation to be within 2% to 10% of the true momentum over the whole p_{T} spectrum and detector acceptance. The corrections are propagated to the measured $\vec{p}_{\mathrm{T}}^{\,\mathrm{miss}}$, which depends on the corrected jets through the clustered tracks. A potential overlap of a jet with the selected lepton is removed in the measurement by ignoring jets that are found within a cone of $\Delta R < 0.4$ around a selected lepton candidate. The analysis considers jets within $|\eta| < 4.7$ whose calibrated transverse energy is greater than 40 GeV with the exception of the HCAL-HF transition region ($2.7 < |\eta| < 3.0$) in which jets must have a transverse momentum of at least 50 GeV to reduce the contribution from detector noise. The event is accepted for further analysis if two or three jets are present.

To reduce the large background from W+jets events, a multivariate analysis (MVA) b tagging algorithm, called cMVA [47], which combines the results from various other b tagging algorithms, is used for identifying jets produced from the hadronisation of b quarks within the acceptance of the silicon tracker ($|\eta| < 2.4$). A tight selection is applied on the discriminant of the algorithm, which gives an efficiency of $\approx 50\%$ for jets originating from true b quarks and a misidentification rate of $\approx 0.1\%$ for light jets from u, d, or s quarks or gluons, as determined from simulation.

Corrections are applied where necessary to the simulated events, to account for known differences relative to data. Lepton trigger, reconstruction, and identification efficiencies are estimated with a "tag-and-probe" method [48] from Z/γ^*+jets data. The b tagging performance in simulation is corrected to match the tagging efficiency observed in data, using scale factors that depend on the p_{T} and η of the selected jets. The scale factors are estimated by dedicated analyses performed with statistically independent selections [47]. A smearing of the jet momenta is applied to account for the known difference in jet energy resolution in simulation compared to data. The profile of pileup interactions is reweighted in simulation to match the one in data derived from the measured instantaneous luminosity. The effects of all these corrections are found to be small.

To classify signal and control regions, different event categories are defined, denoted "NjMb", where N is the total number of selected jets (2 or 3) and M is the number of those jets passing additionally the b tagging requirements (0, 1, or 2). The "2j1b" category is the region with the most sensitivity to the signal yield, whereas the other categories, enriched in background processes with different compositions, are used to assess the background modelling.

A top quark candidate is reconstructed per event in the 2j1b signal region assuming t-channel single top quark production. The procedure commences by first reconstructing the W boson from the selected muon or electron and the missing transverse momentum vector. The p_z component of a neutrino candidate is found by imposing a W boson mass constraint on the system formed by the charged lepton and the missing transverse momentum vector, the latter being interpreted as the projection in the transverse plane of the 4-momentum of the unknown neutrino, as in Ref. [11]. The four-momentum of the top quark candidate (from which its mass, transverse momentum, and rapidity are derived) is then calculated as the vectorial sum of the four-momenta of the charged lepton, the b-tagged jet, and the neutrino candidate. The other, non-tagged jet (j') is then interpreted as originating from the spectator quark, which recoils against the W boson.

4 Multijet estimation

The background from multijet events in the analysis phase space is estimated through a data-driven procedure in two steps. First, templates of the shape of multijet events are obtained from data in a sideband region. Their normalisations are then estimated in a second step through a template-based ML fit to the data in the 2j1b and 3j2b regions simultaneously with the amount of signal events, as described in Section 5. In this section, a dedicated ML fit is performed on events in the 2j0b region only for validating the procedure. The outcome of this ML fit is not used further in the measurement.

In the muon channel, the sideband region is defined by inverting the muon isolation requirement ($I^{\mu}_{\text{rel.}} > 20\%$), which results in a region dominated by multijet events. In the electron channel, the electron candidate is required to fail loose identification criteria, yielding a sideband region consisting not only of antiisolated electrons but also of electrons that fail the photon conversion criteria or are accompanied by large amounts of bremsstrahlung, thus reflecting a combination of various effects. The templates used in the ML fit are determined from this region by subtracting the contamination from other processes from the data, estimated from simulation, which amounts to about 10% (5%) in the muon (electron) channel, respectively.

The template shapes have been validated for various observables in the 2j0b W+jets control region where the fraction of selected multijet events amounts to approximately 10% (20%) for muon (electron) events, respectively, which is comparable to the signal region (see Table 1 below). The transverse W boson mass is calculated from the formula

$$m_{\text{T}}(\text{W}) = 2p_{\text{T}}^{\ell}p_{\text{T}}^{\text{miss}} \cdot \left(1 - \cos(\phi^{\ell} - \phi^{\text{miss}})\right) \tag{3}$$

using the transverse momenta and the azimuthal angles of the charged lepton and the missing momentum. The $m_{\text{T}}(\text{W})$ distributions are shown in Fig. 2 for the muon (left) and electron (right) channel after the multijet templates (extracted from data) and the templates of the processes with prompt leptons (extracted from the simulated events) have been normalised to the result of a dedicated ML fit to data using events in the 2j0b region only. This dedicated fit encompasses only two components, which are the multijet template whose yield is unconstrained in the fit, and all other processes grouped together, with a constraint of $\pm 30\%$ on their combined yield using a log-normal prior. The fit is performed while simultaneously profiling the impact of experimental systematic uncertainties (see Section 8) affecting the yield and shape of the templates. After the fit, the derived multijet templates and the simulated samples in both channels are found to describe the distributions of data well, thus validating the data-driven procedure for estimating the contribution by multijet events. For the measurement, the normalisations of the multijet templates in the 2j1b and 3j2b regions are estimated using a different procedure, as described in Section 5.

5 Signal yield estimation

The number of t-channel single top quark events in data is determined from a ML fit using the distributions of $m_{\text{T}}(\text{W})$ and of two boosted decision tree (BDT) discriminants in the 2j1b region, and the $m_{\text{T}}(\text{W})$ distribution in the 3j2b region. Simultaneously, the background yields and the impact of the experimental systematic uncertainties, modelled using nuisance parameters that influence yield and shape, are profiled.

The first BDT, labelled $\text{BDT}_{t\text{-ch.}}$, has been trained to separate t-channel single top quark events

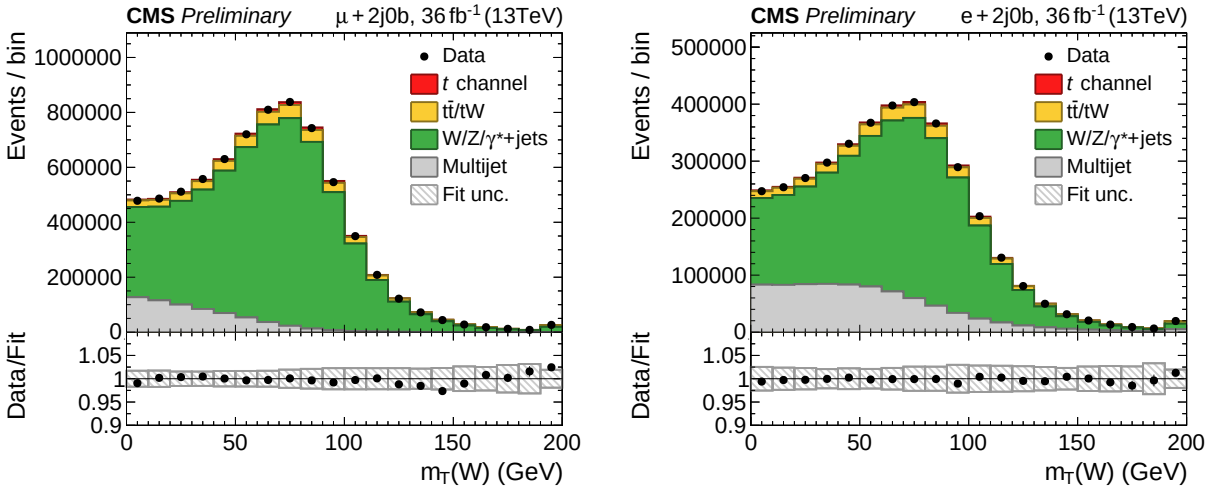

Figure 2: Distributions of the transverse W boson mass in the 2 jets, 0 b-tag control region for the (left) muon and (right) electron channels after scaling the simulated and multijet templates to the result of a dedicated ML fit performed in this region. The lower plots give the ratio of the data to the fit results. The hatched band displays the post-fit uncertainties per bin after the experimental systematic uncertainties have been profiled.

from $\mathrm{t\bar{t}}$, W+jets, and multijet events using corresponding samples of simulated events. The following five observables have been chosen as input:

- the absolute value of the pseudorapidity of the untagged jet, $|\eta(j')|$;
- the reconstructed top quark mass, $m_{\ell\nu\mathrm{b}}$;
- the transverse W boson mass, $m_{\mathrm{T}}(\mathrm{W})$;
- the distance in η-ϕ space ($\Delta R = \sqrt{\Delta\eta^2 + \Delta\phi^2}$) between the untagged jet and the b-tagged jet used to reconstruct the top quark, $\Delta R(\mathrm{b},j')$;
- the absolute difference in pseudorapidity between the selected lepton and the b-tagged jet used to reconstruct the top quark, $|\Delta\eta(\mathrm{b},\ell)|$.

These have been selected based on their sensitivity for separating signal from background events while exhibiting low correlations with the observables used to measure the differential cross sections. The resulting distribution of the $\mathrm{BDT}_{t\text{-ch.}}$ discriminant is presented in Fig. 3 (left).

The $\mathrm{BDT}_{t\text{-ch.}}$ discriminant shapes of the W+jets and $\mathrm{t\bar{t}}$ backgrounds are found to be very similar. To obtain sensitivity in the fit to both backgrounds individually, a second BDT, labelled $\mathrm{BDT}_{\mathrm{t\bar{t}/W}}$, has been trained to classify events only for these two processes using the following six input observables: $m_{\ell\nu\mathrm{b}}$; $p_{\mathrm{T}}^{\mathrm{miss}}$; $\Delta R(\mathrm{b},j')$; $|\Delta\eta(\mathrm{b},\ell)|$; the W boson helicity angle, $\cos\theta^{\star}_{\mathrm{W}}$, defined as the angle between the lepton momentum and the negative of the top quark momentum in the W boson rest frame [22]; and the event shape C, defined using the momentum tensor

$$S^{ab} = \frac{\sum_i^{\mathrm{jets},\,\ell,\,\vec{p}_{\mathrm{T}}^{\,\mathrm{miss}}} p_i^a \cdot p_i^b}{\sum_i^{\mathrm{jets},\,\ell,\,\vec{p}_{\mathrm{T}}^{\,\mathrm{miss}}} |\vec{p}_i|^2} \tag{4}$$

as $C = 3(\lambda_1\lambda_2 + \lambda_1\lambda_3 + \lambda_2\lambda_3)$, where $\lambda_1 + \lambda_2 + \lambda_3 = 1$ and denote the decreasingly-ordered eigenvalues of the momentum tensor S^{ab}. In the two most extreme cases, the event shape

C vanishes for perfectly back-to-back dijet events ($C = 0$) and reaches its maximum ($C = 1$) if the final-state momenta are distributed isotropically. For the measurement, the $\mathrm{BDT}_{\mathrm{t\bar{t}/W}}$ discriminant is evaluated only in a phase space defined by $m_{\mathrm{T}}(\mathrm{W}) > 50$ GeV and $\mathrm{BDT}_{t\text{-ch.}} < 0$, which is found to be largely dominated by background events. Thus, its input observables do not have to be selected explicitly such that they possess low correlation with the observables used to measure the differential cross sections. The resulting $\mathrm{BDT}_{\mathrm{t\bar{t}/W}}$ discriminant distribution is displayed in Fig. 3 (right).

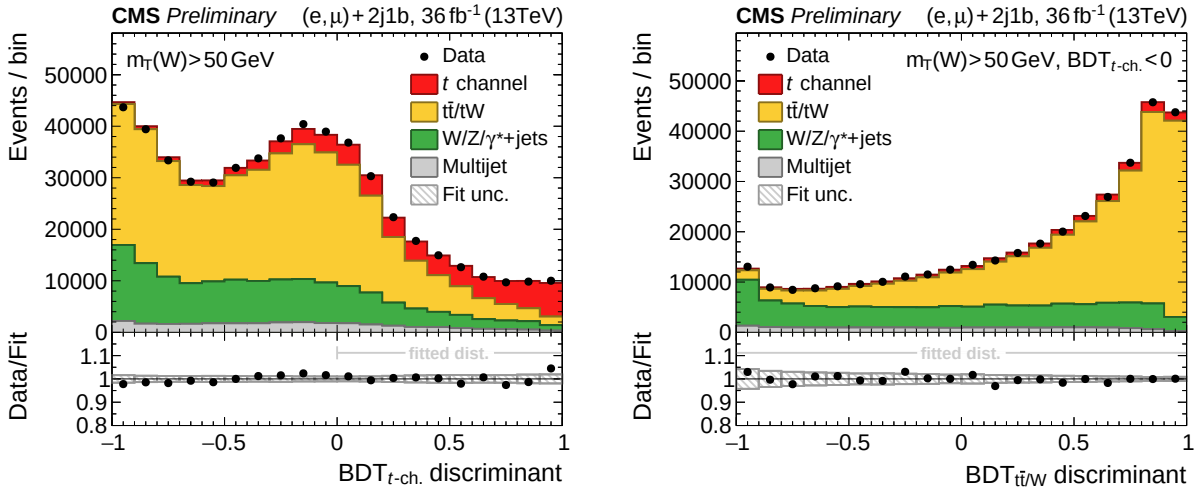

Figure 3: Distributions of the BDT discriminants in 2 jets, 1 b-tag region: (left) $\mathrm{BDT}_{t\text{-ch.}}$ trained to separate signal from background events; (right) $\mathrm{BDT}_{\mathrm{t\bar{t}/W}}$ trained to separate W+jets from $\mathrm{t\bar{t}}$ events in a background-dominated phase space. Events in muon and electron channel have been summed. The predictions have been scaled to the result of the inclusive ML fit. The parts of the distributions used in the fits are indicated in the lower panels. The hatched band displays the post-fit uncertainties per bin after the experimental systematic uncertainties have been profiled.

The ML fit is performed using the following distributions of $m_{\mathrm{T}}(\mathrm{W})$, $\mathrm{BDT}_{\mathrm{t\bar{t}/W}}$, and $\mathrm{BDT}_{t\text{-ch.}}$ from the 2j1b signal region:

- the $m_{\mathrm{T}}(\mathrm{W})$ distribution for events with $m_{\mathrm{T}}(\mathrm{W}) < 50$ GeV, which is particularly sensitive to the amount of multijet events;
- the $\mathrm{BDT}_{\mathrm{t\bar{t}/W}}$ discriminant distribution for events with $m_{\mathrm{T}}(\mathrm{W}) > 50$ GeV and $\mathrm{BDT}_{t\text{-ch.}} < 0$, which defines a region enriched by $\mathrm{t\bar{t}}$ and W+jets but depleted of signal and multijet events;
- the $\mathrm{BDT}_{t\text{-ch.}}$ discriminant distribution for events with $m_{\mathrm{T}}(\mathrm{W}) > 50$ GeV and $\mathrm{BDT}_{t\text{-ch.}} > 0$, which is enriched by signal events.

The $m_{\mathrm{T}}(\mathrm{W})$ distribution in the 2j1b region is shown in Fig. 4 (left). The $m_{\mathrm{T}}(\mathrm{W})$ distribution in the 3j2b control region is included in the fit as well. It provides additional sensitivity to the $\mathrm{t\bar{t}}$ yield, and thus further reduces the correlation between the estimated yields. Its distribution is presented in Fig. 4 (right). In the fit, each distribution is split in two by separating events depending on the reconstructed charge of the selected electron or muon per event. This results in eight distributions per lepton channel and thus 16 distributions in the e/μ combined fit.

The yields of t-channel single top quark and antiquark events are measured independently. Background events containing top quarks ($\mathrm{t\bar{t}}$, tW) are grouped together and only their combined yield is estimated. The top quark background yield is constrained using a log-normal

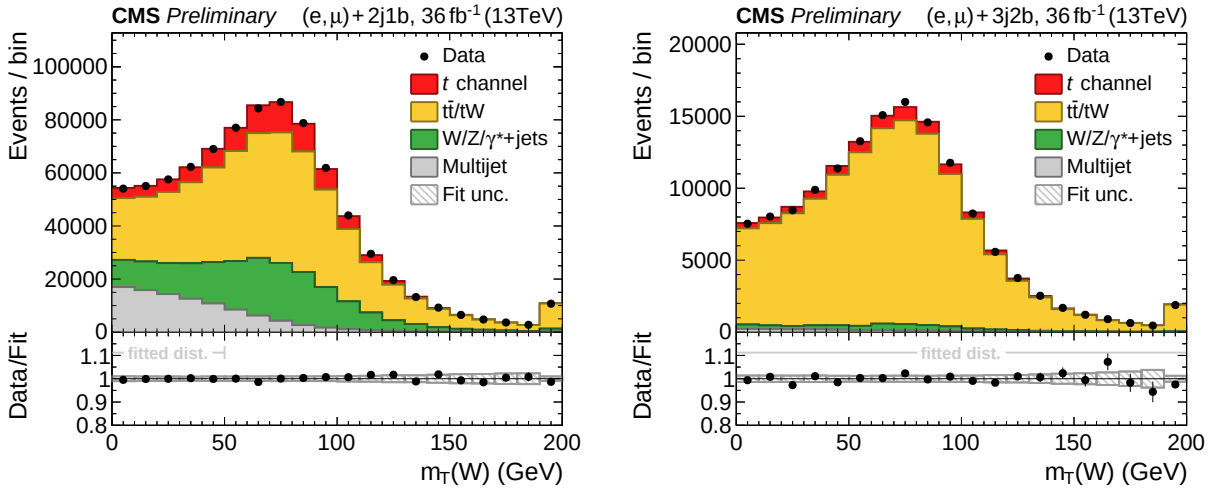

Figure 4: Distributions of the transverse W boson mass (left) for events with 2 jets, 1 b-tag and (right) in events with 3 jets, 2 b-tags. Events in muon and electron channel have been summed. The predictions have been scaled to the result of the inclusive ML fit. The parts of the distributions used in the fits are indicated in the lower panels. The hatched band displays the post-fit uncertainties per bin after the experimental systematic uncertainties have been profiled.

prior with a width of $\pm 10\%$ to account for the uncertainty in the theoretical $t\bar{t}$ and tW production cross sections and also to account for the uncertainty when two out of the four jets expected from semileptonic $t\bar{t}$ production are not within acceptance, as it is the case in the 2j1b region. The electroweak background processes, W+jets and Z/γ^*+jets, are grouped together as well, and a conservative uncertainty of $\pm 30\%$ in their combined yield is applied using a log-normal prior constraint. This is motivated by the theoretical uncertainty in the modelling of the W and Z/γ^* production rates in association with two or more (heavy-flavoured) jets [49, 50]. The yields of multijet events are assumed to be independent per lepton type and region. Their yields are constrained by a log-normal prior with a width of $\pm 100\%$ with respect to the template normalisations obtained from data in the sideband regions. In addition, a conservative uncertainty in the predicted lepton charge ratio per background process is taken into account using a Gaussian prior with a width of $\pm 1\%$ in the fit. The impact of the finite number of simulated events on the templates is accounted for by employing the so-called "Barlow-Beeston-lite" method [51].

Experimental systematic uncertainties (described in Section 8) are profiled in the fit simultaneously with the yields and charge ratios. Each source is assigned a nuisance parameter according to which the shape and yield of the fit templates are modified.

The resulting event yields from a simultaneous fit to the data in the electron and muon channels are presented in Table 1. Overall, the distributions used in the fit, shown in Figs. 3 and 4, are found to be well modelled by the samples of simulated events and the data-driven multijet templates after normalising them to the fit result.

For the differential cross section measurements, individual fits are performed for each observable that is later used in the unfolding (see Section 7). In each fit, the signal and background yields can vary independently across the intervals of the corresponding observable. The likelihood L to be maximised in such fits can be expressed as

Table 1: Measured and observed event yields in the 2j1b region for each lepton channel and charge. The uncertainties in the yields denote the post-fit uncertainties per process after the experimental systematic uncertainties have been profiled.

Process	e^+	e^-	μ^+	μ^-
$W/Z/\gamma^*$+jets	$33\,400 \pm 3\,200$	$30\,700 \pm 2\,800$	$72\,000 \pm 6\,800$	$62\,800 \pm 5\,600$
$t\bar{t}$/tW	$84\,500 \pm 1\,400$	$84\,800 \pm 1\,500$	$142\,400 \pm 2\,400$	$143\,400 \pm 2\,500$
Multijet	$13\,500 \pm 1\,000$	$12\,700 \pm 1\,000$	$35\,150 \pm 550$	$35\,710 \pm 760$
t channel (top quark)	$17\,720 \pm 820$	27 ± 2	$34\,400 \pm 1500$	10 ± 3
t channel (top antiquark)	25 ± 3	$11\,460 \pm 880$	13 ± 2	$21\,600 \pm 1\,600$
Total	$149\,300 \pm 2\,400$	$139\,700 \pm 2\,200$	$284\,100 \pm 5\,800$	$263\,700 \pm 4\,600$
Data	148 400	138 700	283 300	260 000

$$\ln\left(L(\vec{\beta},\vec{\nu},\vec{R})\right) = -\sum_{k}^{\text{region}}\sum_{j}^{\text{int. bins}}\sum_{i}\left(d_{kji}\cdot\ln p_{kji}(\vec{\beta}_j,\vec{\nu},\vec{R}) - p_{kji}(\vec{\beta}_j,\vec{\nu},\vec{R})\right) + \text{constraints}\,, \quad (5)$$

where d denotes the number of events observed in data and p the estimated prediction. The summation over k denotes the 16 regions (four observables $\times$ lepton channel $\times$ lepton charge), j denotes the interval in the unfolding observable, and i denotes a bin in one of the distributions. The prediction $\vec{p}_{kj}$, which includes all bins i for interval j and region k is given by

$$\begin{aligned}\vec{p}_{kj}(\vec{\beta}_j,\vec{\nu},\vec{R}) = {} & \beta_{\mathrm{t},j}\cdot\vec{T}^{t\text{-ch.}}_{\mathrm{t},kj}(\vec{\nu}) + \beta_{\bar{\mathrm{t}},j}\cdot\vec{T}^{t\text{-ch.}}_{\bar{\mathrm{t}},kj}(\vec{\nu}) \\ & + \beta_{\mathrm{t\bar{t}/tW},j}\cdot\vec{T}^{\mathrm{t\bar{t}/tW}}_{kj}(R_j,\vec{\nu}) + \beta_{\mathrm{W/Z/\gamma^*+jets},j}\cdot\vec{T}^{\mathrm{W/Z/\gamma^*+jets}}_{kj}(R_j,\vec{\nu}) \\ & + \beta_{\mathrm{multijet},kj}\cdot\vec{T}^{\mathrm{multijet}}_{kj}(R_{kj},\vec{\nu})\,, \end{aligned} \quad (6)$$

where β_X are the normalisations of the templates $\vec{T}_X$, $\vec{\nu}$ are the nuisance parameters, and R_X are the charge ratios of each background process. The profiling of systematic uncertainties leads to a correlation between the t-channel top quark and antiquark yields in the same interval of about 20–30%. These correlations are propagated to the differential cross sections for each top quark charge and are accounted for when calculating their sum and ratio.

Since the kinematic selection of electrons events is restricted to $p_{\mathrm{T}} > 35$ GeV and $|\eta| < 1.479$, which is tighter than for muon events ($p_{\mathrm{T}} > 26$ GeV, $|\eta| < 2.4$), the signal yields in the lowest interval of the lepton p_{T} and in the highest two intervals of the lepton $|\eta|$ spectra are estimated using solely distributions from the muon channel in the combined e/μ fit.

6 Validation of signal and background modelling

The distributions of the unfolding observables are validated in a background-dominated and in a signal-enriched phase space before unfolding. Both regions are defined for events in the 2j1b category that also satisfy $m_{\mathrm{T}}(\mathrm{W}) > 50$ GeV to suppress the contribution from multijet production. The modelling of the $t\bar{t}$/tW and $W/Z/\gamma^*$+jets backgrounds is validated in a background-dominated region obtained from events having $\mathrm{BDT}_{t\text{-ch.}} < 0.0$. To validate the modelling of the t-channel process, events are instead required to pass $\mathrm{BDT}_{t\text{-ch.}} > 0.7$, resulting in a sample enriched in signal events. These two regions and their selections are only defined and applied

for validation purposes and not used for measuring the differential cross sections for which the individual fit results are used in the unfolding instead.

The resulting distributions in both regions for all six unfolding observables are shown in Figs. 5 and 6 after the predictions have been scaled to the inclusive fit result. Overall good agreement between data and the fit result is observed in the background-dominated phase space thus validating the modelling of the $\mathrm{t\bar{t}}$/tW and W/Z/γ^*+jets backgrounds. In the signal region, reasonable agreement is also observed, except for the top quark p_T distribution, which has some deviations with respect to the fit uncertainties shown in the figures.

7 Unfolding

The aim of this analysis is to measure the parton- and particle-level differential cross sections of t-channel single top quark production as a function of the single top quark transverse momentum, rapidity, and polarisation angle, the lepton transverse momentum and rapidity, and the transverse momentum of the W boson from the top quark decay. The distributions from reconstructed events are affected by detector resolution, selection efficiencies and kinematic reconstruction, which lead to distortions with respect to the corresponding distributions at the parton or particle levels. The size of these effects varies with the event kinematics. In order to correct for these effects and determine the parton- and particle-level distributions, an unfolding method is applied to the reconstructed distributions. In this analysis, the TUNFOLD algorithm [52] is chosen, which treats unfolding as a minimisation problem of the function

$$\chi^2 = (\vec{y} - \boldsymbol{R}\boldsymbol{\epsilon}\vec{x})^\mathrm{T}\, \boldsymbol{V}_y^{-1}\, (\vec{y} - \boldsymbol{R}\boldsymbol{\epsilon}\vec{x}) + \underbrace{\tau^2\, \|\boldsymbol{L}(\vec{x} - \vec{x}_0)\|^2}_{\text{regularisation}} + \lambda \sum_i (\vec{y} - \boldsymbol{R}\boldsymbol{\epsilon}\vec{x})_i \,, \tag{7}$$

where $\vec{y}$ denotes the measured yields in data, $\boldsymbol{V}_y$ the covariance matrix of the measured yields, and $\vec{x}$ the corresponding differential cross section at parton or particle level. The matrices $\boldsymbol{R}$ and $\boldsymbol{\epsilon}$ denote the transition probabilities and selection efficiencies estimated from simulation, respectively. The signal yields and covariances are estimated through ML fits using the $m_\mathrm{T}(\mathrm{W})$, $\mathrm{BDT}_{\mathrm{t\bar{t}/W}}$, and $\mathrm{BDT}_{t\text{-ch.}}$ distributions, as detailed in Section 5.

A penalty term, based on the curvature of the unfolded spectrum [53, 54] encoded in the matrix $\boldsymbol{L}$, is added in the minimisation to suppress oscillating solutions originating from amplified statistical fluctuations. This procedure is called "regularisation" and its strength τ is chosen so as to minimise the global correlation between the unfolded bins. The so-called "bias vector" $\vec{x}_0$ is set to the expected spectrum from simulation. Pseudo-experiments using simulated data are performed to verify that the unfolding method estimates the uncertainties correctly while keeping the regularisation bias at a minimum. No regularisation is applied when unfolding the lepton p_T and rapidity spectra since the migrations between bins is found to be very small. The overall normalisation of the unfolded spectrum is determined by performing a simultaneous minimisation with respect to the Lagrange parameter λ.

The parton-level top quark is defined as the generated on-shell top quark after QED and QCD radiation, taking into account the intrinsic k_T of initial-state partons. Events are required to contain either a muon or electron from the top quark decay chain. This also includes muons or electrons from intermediately produced tau leptons. In such events, the W boson is chosen to be the direct daughter of the top quark. The spectator quark is selected from among the light quarks after QED and QCD radiation that are not products of the top quark decay. In case of ambiguities arising from initial-state radiation, the spectator quark that minimises the

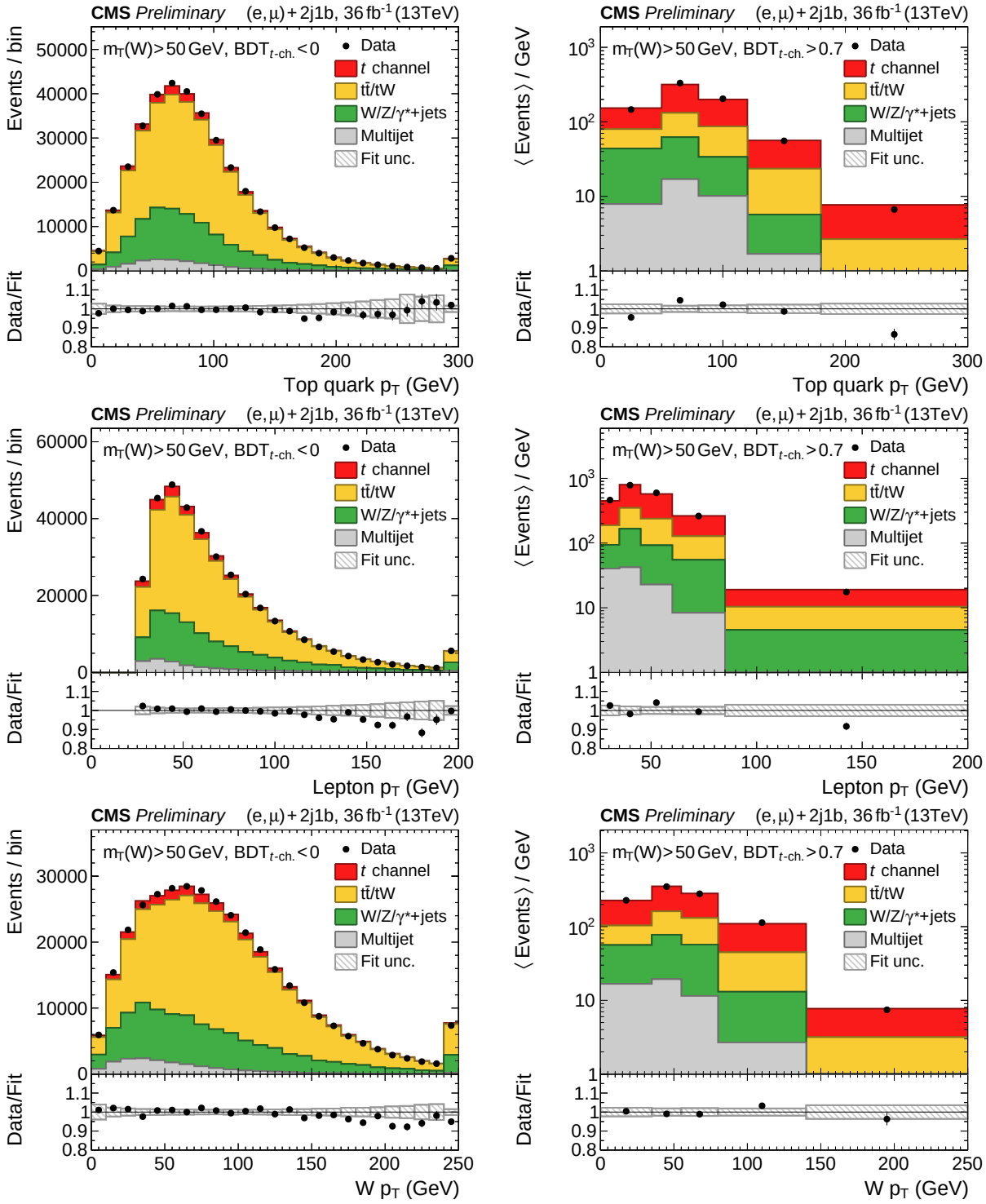

Figure 5: Distributions of the unfolding observables in a (left column) background-dominated and a (right column) signal-enriched region for events passing the 2 jets, 1 b-tag selection: (upper row) top quark p_T; (middle row) charged lepton p_T; (lower row) W boson p_T. Events in muon and electron channel have been summed. The predictions have been scaled to the result of the inclusive ML fit. The lower plots give the ratio of the data to the fit results. The hatched band displays the post-fit uncertainties per bin after the experimental systematic uncertainties have been profiled.

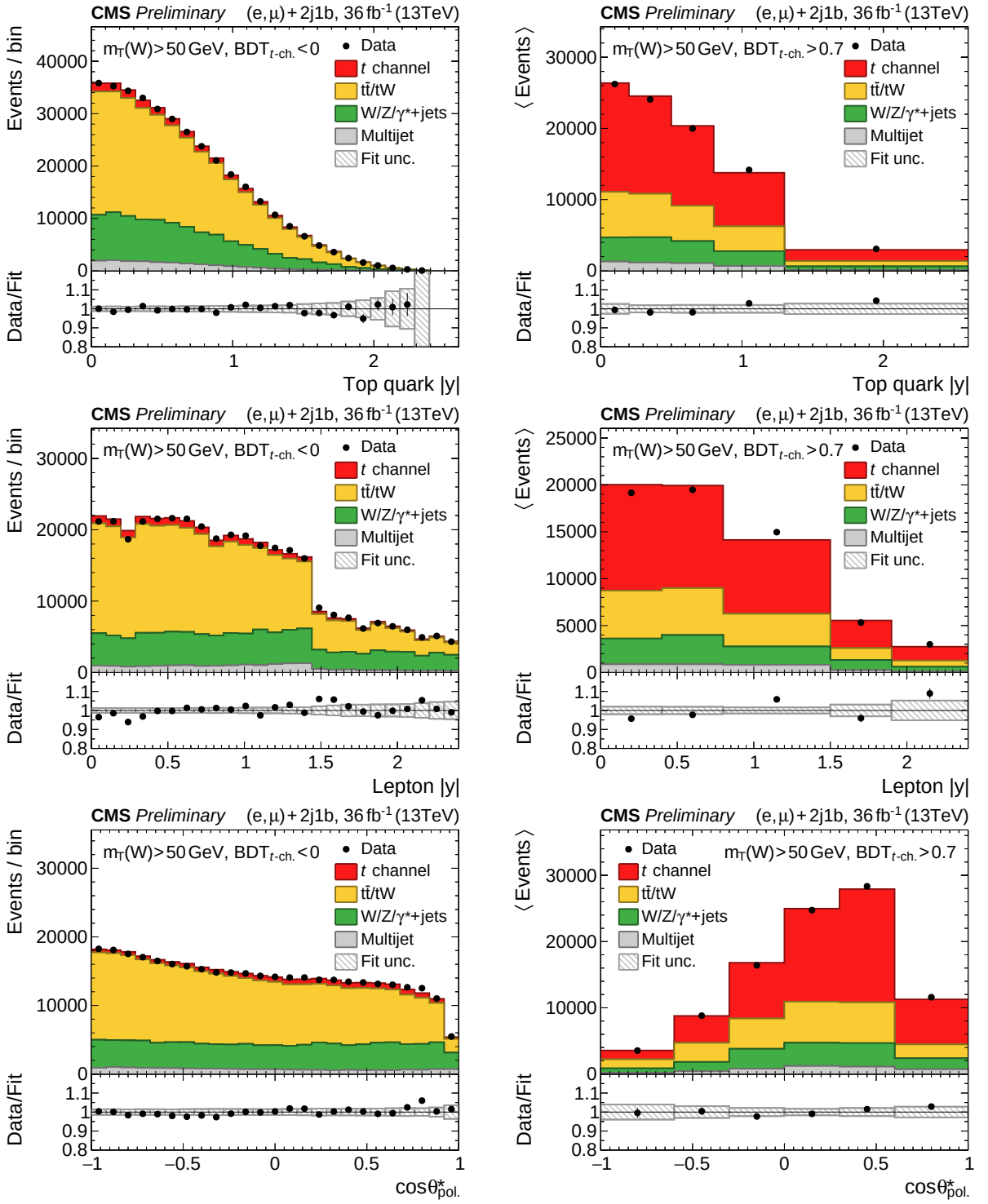

Figure 6: Distributions of the unfolding observables in a (left column) background-dominated and a (right column) signal-enriched region for events passing the 2 jets, 1 b-tag selection: (upper row) top quark rapidity; (middle row) charged lepton rapidity; (lower row) top quark polarisation angle. Events in muon and electron channel have been summed. The predictions have been scaled to the result of the inclusive ML fit. The lower plots give the ratio of the data to the fit results. The hatched band displays the post-fit uncertainties per bin after the experimental systematic uncertainties have been profiled.

transverse momentum of the combined spectator quark and top quark system is chosen.

The top quark at particle level (called "pseudo top quark") is defined in simulated events by performing an event reconstruction based on the set of stable simulated particles after hadronisation [25]. In the context of this study, all particles with a lifetime of more than 30 ps are considered stable. So-called "dressed" electrons and muons are constructed by accounting for the additional momenta carried by photons within a cone of $\Delta R < 0.1$ around the corresponding prompt lepton that do not originate from hadronisation products. The missing transverse momentum vector is defined as the summed momentum of all prompt neutrinos in the event. Jets at parton level are clustered from all stable particles excluding prompt electrons, prompt muons, prompt photons, and all neutrinos using the anti-k_{T} algorithm with a distance parameter of $R = 0.4$. From these objects a pseudo top quark is reconstructed by first solving for the unknown neutrino p_z momentum, which is identical to the top quark reconstruction procedure apply to data, as described in Section 3. Events containing a single dressed electron or muon with $p_{\mathrm{T}} > 26$ GeV and $|\eta| < 2.4$, together with two jets with $p_{\mathrm{T}} > 40$ GeV and $|\eta| < 4.7$, are considered at particle level. Jets that are closer than $\Delta R = 0.4$ to the selected dressed muon or electron are ignored. The jet that yields a top quark mass closest to 172.5 GeV is assumed to come from the top quark decay, while the other jet is taken as the spectator jet.

The binning is chosen so as to minimise the migrations between the reconstructed bins while retaining sensitivity to the shapes of the distributions. The stability (purity) is defined as the probability that the parton- or particle-level (reconstructed) values of an observable within a certain range also have their reconstructed (parton-/particle-level) counterparts in the same range. Both quantities are found to be greater than or equal to 50% in most bins of all distributions, with the exception of a few bins at parton level where those drop to 40%, and the first two bins of the polarisation angle distribution at parton level where both quantities drop to about 25%. The stability and purity values are about 10% larger for the particle-level distributions than for the parton-level ones. The acceptance for selecting t-channel single top quark events is measured to be in the range 1–5% (10–20%) for electron events and 2–8% (20–30%) for muon events at parton (particle) level, respectively.

8 Systematic uncertainties

The measurements are affected by various sources of systematic uncertainty. For each systematic variation new templates and response matrices are derived. Systematic variations can create (anti)correlations between the t-channel top quark and antiquark yields since both yields are estimated simultaneously from data through an ML fit, as described in Section 5.

The following experimental systematic uncertainties are profiled in the ML fit.

Background composition As described in Section 5, the Z/γ^*+jets and W+jets processes and the $\mathrm{t\bar{t}}$ and tW processes are separately grouped together in the ML fit. The ratios of the Z/γ^*+jets to the W+jets yields and the $\mathrm{t\bar{t}}$ to the tW yields are assigned a $\pm 20\%$ uncertainty. This covers the uncertainty in the small Z/γ^*+jets and tW yields for which the analysis has little sensitivity.

Multijet shape estimation The multijet event distributions are estimated from data by inversion of the muon isolation criterion or the electron identification criteria. The uncertainty in the shape of the distributions is estimated by varying the criteria. The requirement on the muon isolation parameter in the sideband region is modified from $I^{\mu}_{\mathrm{rel.}} > 20\%$ to either $20 < I^{\mu}_{\mathrm{rel.}} < 40\%$ or $I^{\mu}_{\mathrm{rel.}} > 40\%$, and the electron isolation parameter to either $I^{e}_{\mathrm{rel.}} < 30\%$

or $I^{e}_{\text{rel.}} > 5.88\%$ while inverting the identification criteria. Another variation is done by requiring electrons in the sideband region to explicitly pass or fail the photon conversion criterion, which is also part of the electron identification requirement.

B tagging and misidentification efficiency The scale factors used to reweight the b tagging and misidentification efficiencies in simulation to the ones estimated from data are varied within their uncertainties based on the true flavour of the selected jets [47].

Jet energy scale and resolution The jet energy scale and resolution corrections are varied within their uncertainties [55]. The shifts induced in the jet momenta are propagated to the missing transverse momentum as well.

Unclustered energy The contributions to $p_{\text{T}}^{\text{miss}}$ of PF candidates that have not been clustered into jets are varied within their respective energy resolutions [56].

Pileup The simulated distribution of pileup interactions is modified by shifting the effective inelastic pp cross section by $\pm 5\%$ [57].

Lepton efficiencies Scale factors that account for differences in the lepton selection and reconstruction efficiencies between data and simulation are varied within their uncertainties [27, 58].

The systematic uncertainties in the theoretical predictions from the simulation are estimated by modifying each input parameter within its uncertainty, producing new simulated events, and using the maximum difference with the nominal prediction as the estimated uncertainty. This is added in quadrature to the uncertainty. The following sources of theoretical uncertainty have been evaluated.

Modelling of top quark p_{T} in $\text{t}\bar{\text{t}}$ events Differential $\text{t}\bar{\text{t}}$ cross section measurements by CMS [59, 60] have shown that the p_{T} spectrum of top quarks in $\text{t}\bar{\text{t}}$ events is significantly softer than predicted by NLO simulations. To correct for this effect, simulated $\text{t}\bar{\text{t}}$ events are reweighted according to scale factors derived from measurements at 13 TeV. The difference in the predictions from using the default $\text{t}\bar{\text{t}}$ simulation sample is taken as an additional uncertainty.

Top quark mass The nominal top quark mass of 172.5 GeV is modified by ± 0.5 GeV in the simulation and the effect is propagated through the unfolding procedure. The difference with respect to the nominal simulation results is taken as the corresponding uncertainty.

Parton distribution function The effect of the uncertainty in the PDFs is estimated by reweighting the simulated events using the recommended variations in the NNPDF3.0 set, including a variation of the strong coupling constant [39]. The reweighting is performed using precomputed weights stored in the event record by the matrix element generator [61].

Renormalisation/factorisation scales A reweighting procedure similar to that used for the PDFs is carried out on simulated *t*-channel, W+jets, and $\text{t}\bar{\text{t}}$ simulated events to estimate the effect of the uncertainties in the renormalisation and factorisation scales. The weights correspond to independent variations by factors of 0.5 and 2 in the scales with respect to their nominal values. The envelope of all possible combinations of up-varied/down-varied scales with the exception of the extreme up/down combinations is considered as an uncertainty. This uncertainty is evaluated independently for the *t*-channel, W+jets, and $\text{t}\bar{\text{t}}$ simulated event samples.

Parton shower Uncertainties in the parton shower simulation are evaluated by comparing the nominal samples to dedicated samples with varied shower parameters. For t-channel single top quark production, the differences with respect to samples with a varied factorisation scale by a factor of 2 or 0.5 or with a varied h_{damp} parameter are taken as two independent uncertainties. For simulated $\mathrm{t\bar{t}}$ samples, the variation of the factorisation scale in both initial- and final-state radiation and the h_{damp} parameter are evaluated as three independent uncertainties.

Underlying event tune The impact of uncertainties arising from the CUETP8M2T4 tune [34] used in the simulation of $\mathrm{t\bar{t}}$ events is evaluated using dedicated samples with the tune varied within its uncertainties.

In addition, an uncertainty of $\pm 2.5\%$ in the measurement of the integrated luminosity of the analysed data set [26] is taken into account by scaling the evaluated covariance matrix per observable accordingly.

9 Results

The differential cross sections of t-channel single top quark production as a function of the top quark transverse momentum, rapidity, and polarisation angle, the transverse momentum and rapidity of the charged lepton (electron or muon) that originates from the top quark decay, and the transverse momentum of the W boson from the top quark decay are presented in Figs. 7 and 8 at the parton and particle levels, respectively. The normalised differential cross sections of the same observables at parton and particle level are provided in Figs. 9 and 10. The differential cross sections refer to t-channel single top quark production where the top quark decays leptonically (into either muon or electron) including events where the charged lepton stems from an intermediate tau lepton decay. The results are compared to the predictions by the POWHEG generator interfaced with PYTHIA 8 in 4FS and the MG5_aMC@NLO generator interfaced with PYTHIA 8 in 4FS and 5FS. An overall good agreement of the results with the predictions in 4FS is observed except for a slight deviation at low top quark transverse momenta. The predictions in 5FS for the top quark and W boson transverse momenta distributions are less in agreement with the data.

Differential ratios of the top quark production rates to the sum of the top quark and antiquark rates as a function of the top quark transverse momentum and rapidity, the transverse momentum and rapidity of the charged lepton, and the W boson transverse momentum are presented in Figs. 11 and 12 at parton and particle level, respectively. It is found that the standard definition of the charge ratio in the literature, i.e. $\sigma_{\mathrm{t}}/\sigma_{\bar{\mathrm{t}}}$, can yield large variances when the precision in certain intervals of the differential cross section for the top antiquark is low. Therefore, the charge ratio is defined as $\sigma_{\mathrm{t}}/\sigma_{\mathrm{t}+\bar{\mathrm{t}}}$ in this note. The ratios have been calculated from the measured cross sections at parton and particle level, respectively, while accounting for correlations between the top quark and antiquark spectra, as detailed in Sections 5 and 8. The resulting charge ratios are compared to the predictions by the NNPDF3.0, MMHT14 [62], and CT10 PDF sets, which have been calculated using the POWHEG signal sample—generated in 4FS and interfaced with PYTHIA 8. The uncertainty bands shown in Figs. 11 and 12 represent the total uncertainty from varying the corresponding PDF eigenvectors and the strong coupling constant. Within the uncertainties, the measured charge ratios are in good agreement with the predictions from all three PDF sets.

The spin asymmetry, sensitive to the top quark polarisation, is determined from the spectrum of the differential cross section as a function of the polarisation angle at parton level (Fig. 7,

lower right). A linear χ^2-based fit, assuming the expected functional dependence given in Equation 2, is used to take the correlations between the unfolded bins into account. The spin asymmetry is measured to be

$$A_e = 0.443 \pm 0.048\,(\text{stat+exp}) \pm 0.068\,(\text{syst}) = 0.443 \pm 0.083\,, \tag{8}$$

$$A_\mu = 0.398 \pm 0.042\,(\text{stat+exp}) \pm 0.047\,(\text{syst}) = 0.398 \pm 0.063\,, \tag{9}$$

$$A_{e+\mu} = 0.439 \pm 0.032\,(\text{stat+exp}) \pm 0.053\,(\text{syst}) = 0.439 \pm 0.062\,, \tag{10}$$

for electron, muon, and combined events, respectively. The first uncertainty, labelled "stat+exp", denotes the post-fit uncertainties after the experimental systematic uncertainties have been profiled, whereas the latter one, labelled "syst", is the theoretical systematic uncertainty. The measured asymmetries are in good agreement with the predicted SM value of 0.436, found using POWHEG at NLO, with a very small uncertainty. In particular the deviation observed in a previous analysis using pp collision data at a centre-of-mass energy of 8 TeV corresponding to 2.0 standard deviations [17] is not strengthened further.

10 Summary

Differential cross sections for *t*-channel single top quark production in proton-proton collisions at a centre-of-mass energy of 13 TeV have been measured by the CMS experiment at the LHC using a sample of proton-proton collision events, corresponding to an integrated luminosity of 36 fb^{-1}. The cross sections are determined as a function of the top quark transverse momentum, rapidity, and polarisation angle, the charged lepton transverse momentum and rapidity, and the transverse momentum of the W boson from the top quark decay. In addition, the differential charge ratio $\sigma_t/\sigma_{t+\bar{t}}$ has been measured as a function of the top quark transverse momentum and rapidity, the charged lepton transverse momentum and rapidity, and the transverse momentum of the W boson from the top quark decay. Data events containing a single electron or muon and two or three jets are used. The single top quark and antiquark yields are determined through maximum-likelihood fits to the data distributions. The differential cross sections are then found at the parton and particle levels by unfolding estimated signal yields. The results are compared to various next-to-leading order (NLO) predictions and found to be in good agreement. Also, the differential charge ratios are compared against various parton distribution function sets and all are found within uncertainties. Lastly, the top quark spin asymmetry, which is sensitive to the top quark polarisation, has been measured using the differential cross section as a function of the top quark polarisation angle at the parton level. The measured spin asymmetry value of 0.439 ± 0.062 is in good agreement with the standard model prediction, found using the POWHEG event generator at NLO.

References

[1] M. Aliev et al., "HATHOR: HAdronic Top and Heavy quarks crOss section calculatoR", *Comput. Phys. Commun.* **182** (2011) 1034, doi:10.1016/j.cpc.2010.12.040, arXiv:1007.1327.

[2] P. Kant et al., "HATHOR for single top-quark production: Updated predictions and uncertainty estimates for single top-quark production in hadronic collisions", *Comput. Phys. Commun.* **191** (2015) 74, doi:10.1016/j.cpc.2015.02.001, arXiv:1406.4403.

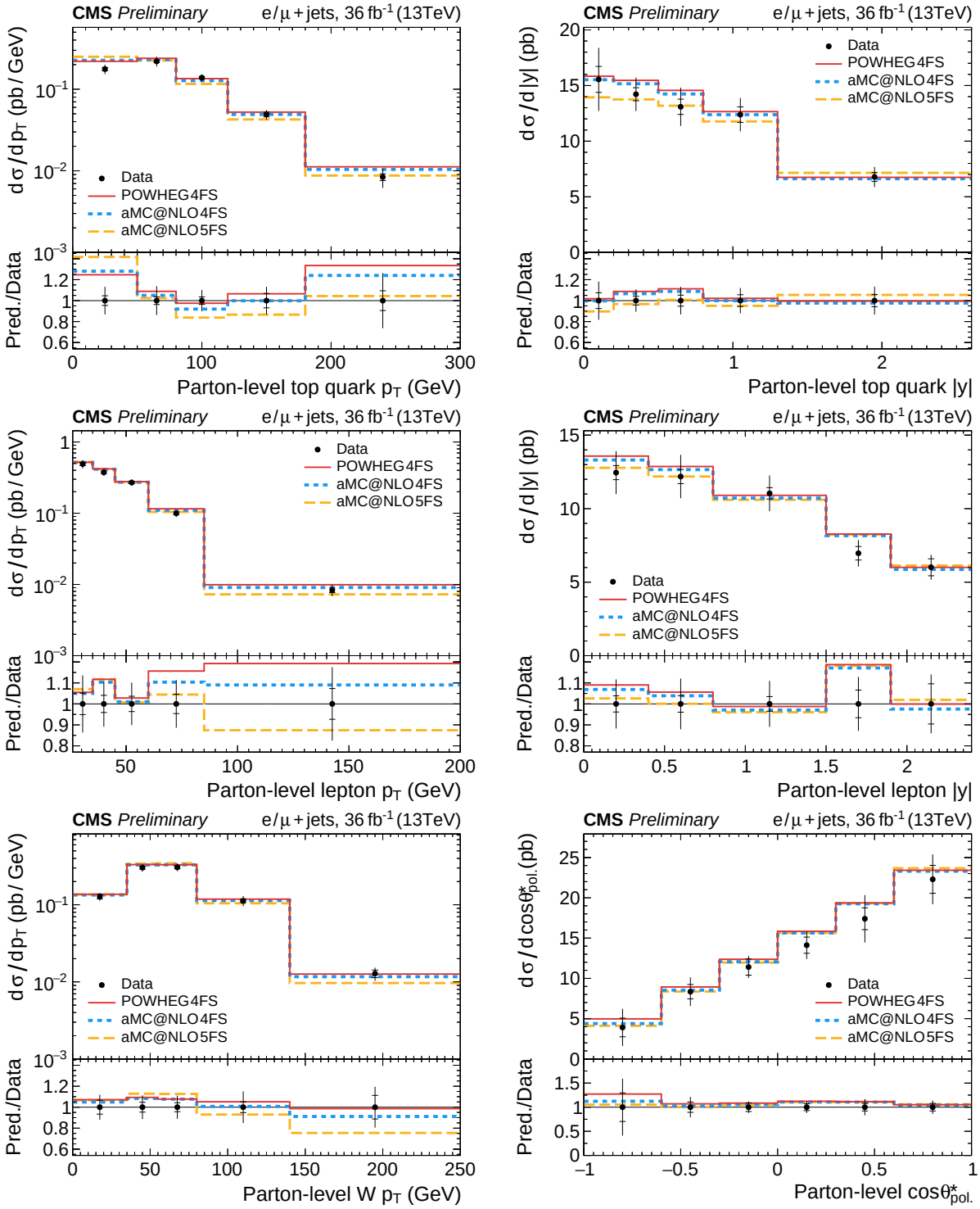

Figure 7: Differential t-channel single top quark cross sections at parton level: (upper row) top quark p_T and rapidity; (middle row) charged lepton p_T and rapidity; (lower left) W boson p_T; (lower right) top quark polarisation angle. The inner tick marks denote the unfolded post-fit uncertainty after the experimental systematic uncertainties have been profiled.

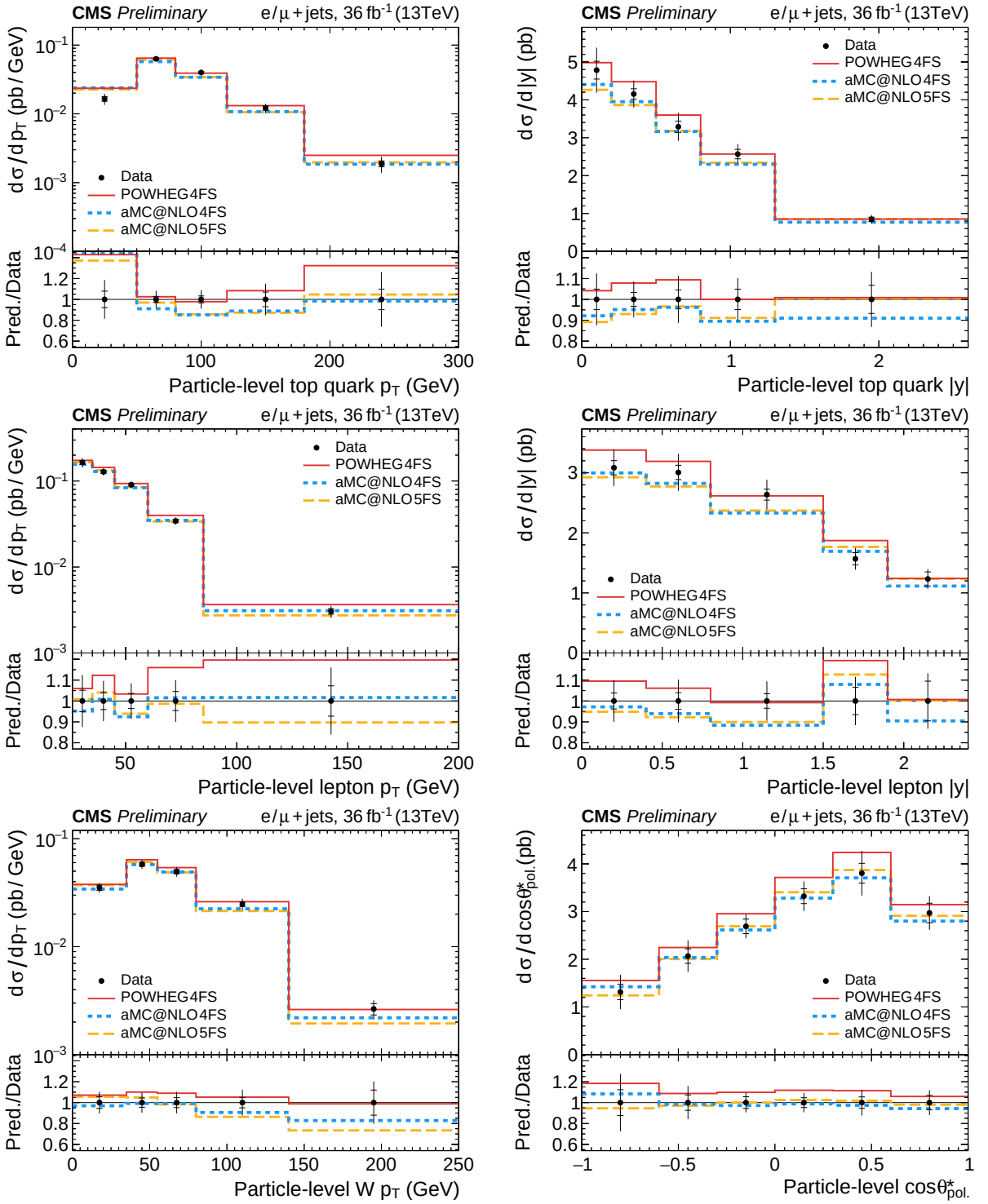

Figure 8: Differential t-channel single top quark cross sections at particle level: (upper row) top quark p_{T} and rapidity; (middle row) charged lepton p_{T} and rapidity; (lower left) W boson p_{T}; (lower right) top quark polarisation angle. The inner tick marks denote the unfolded post-fit uncertainty after the experimental systematic uncertainties have been profiled.

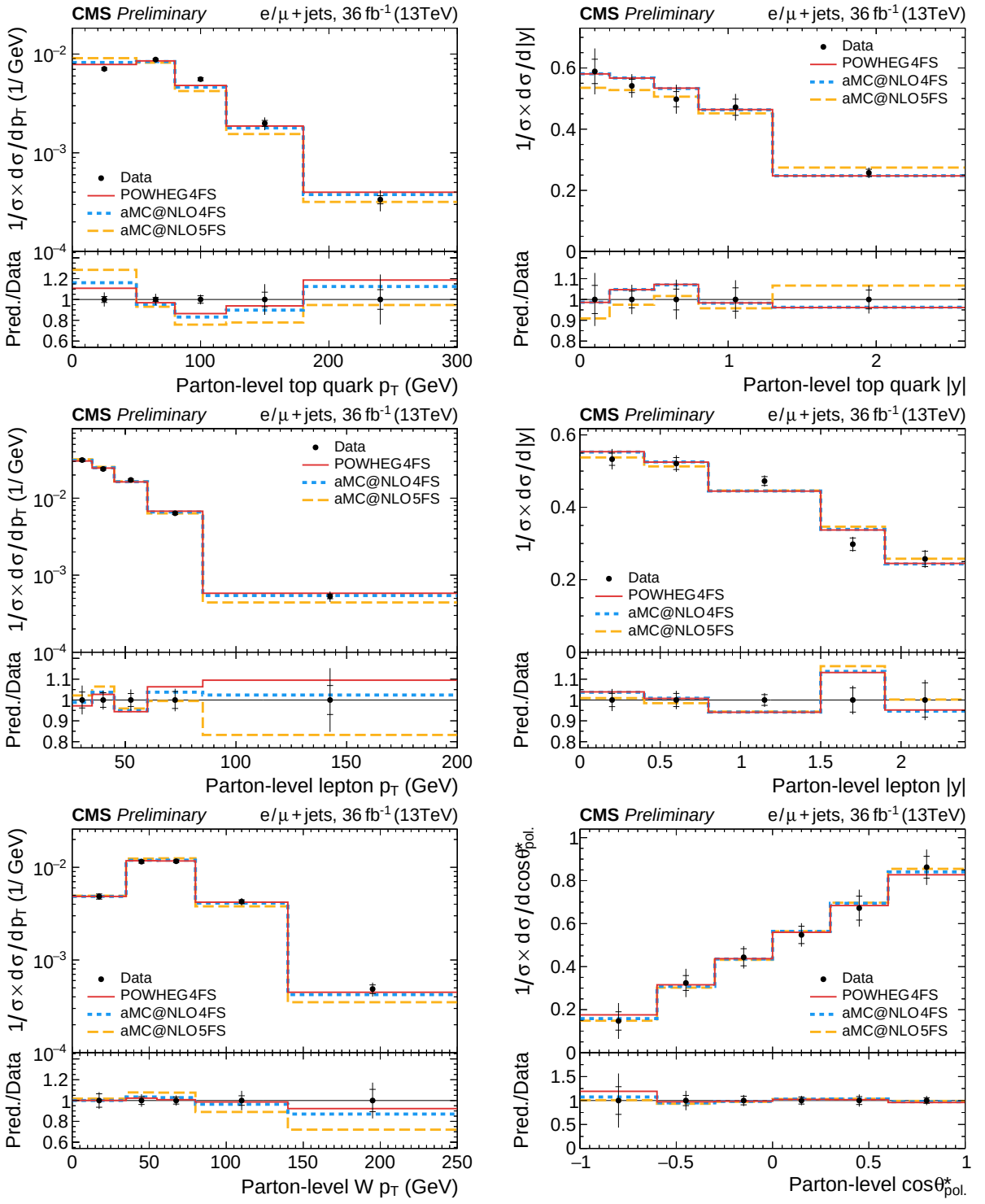

Figure 9: Normalised differential t-channel single top quark cross sections at parton level: (upper row) top quark p_{T} and rapidity; (middle row) charged lepton p_{T} and rapidity; (lower left) W boson p_{T}; (lower right) top quark polarisation angle. The inner tick marks denote the unfolded post-fit uncertainty after the experimental systematic uncertainties have been profiled.

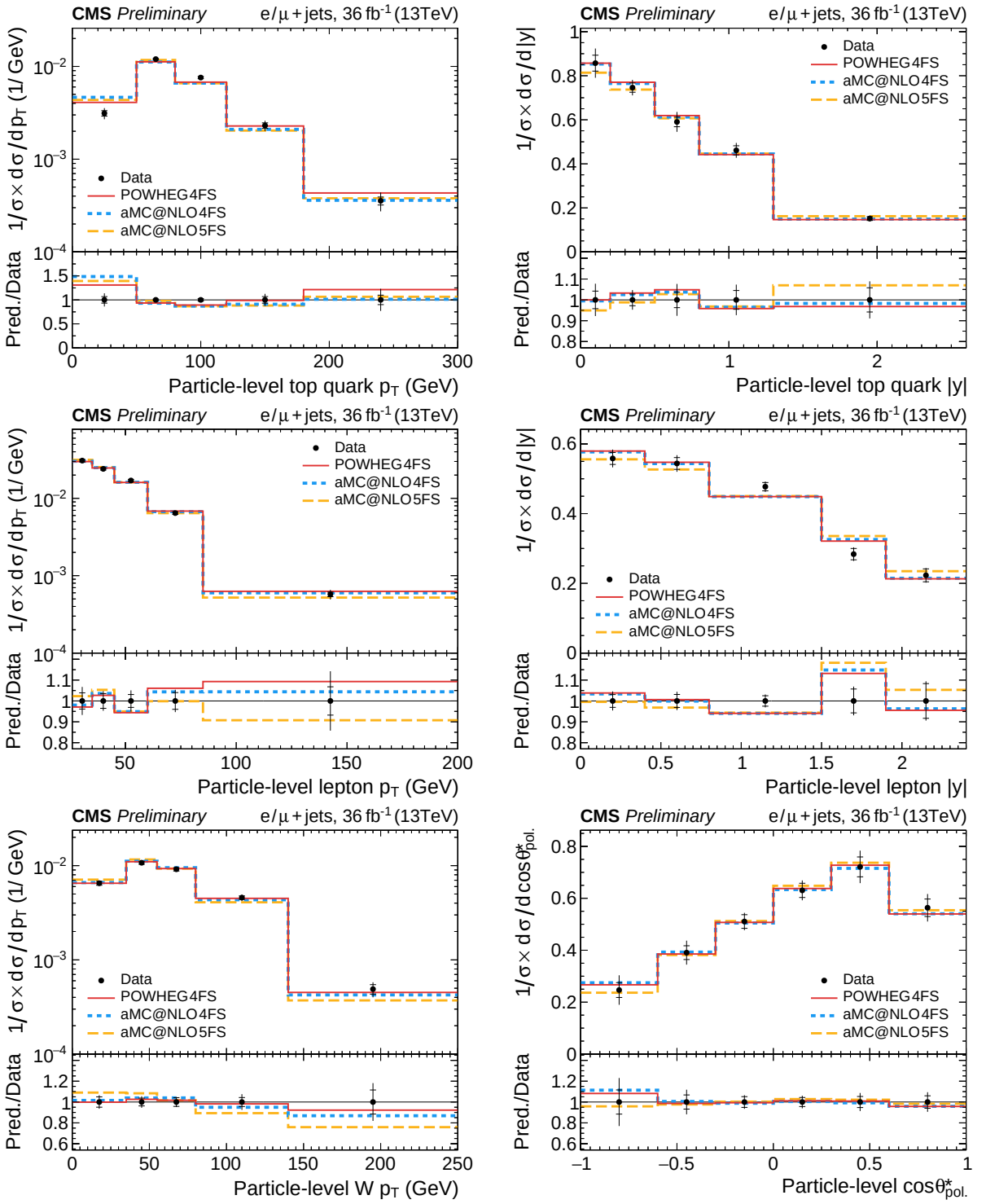

Figure 10: Normalised differential t-channel single top quark cross sections at particle level: (upper row) top quark p_{T} and rapidity; (middle row) charged lepton p_{T} and rapidity; (lower left) W boson p_{T}; (lower right) top quark polarisation angle. The inner tick marks denote the unfolded post-fit uncertainty after the experimental systematic uncertainties have been profiled.

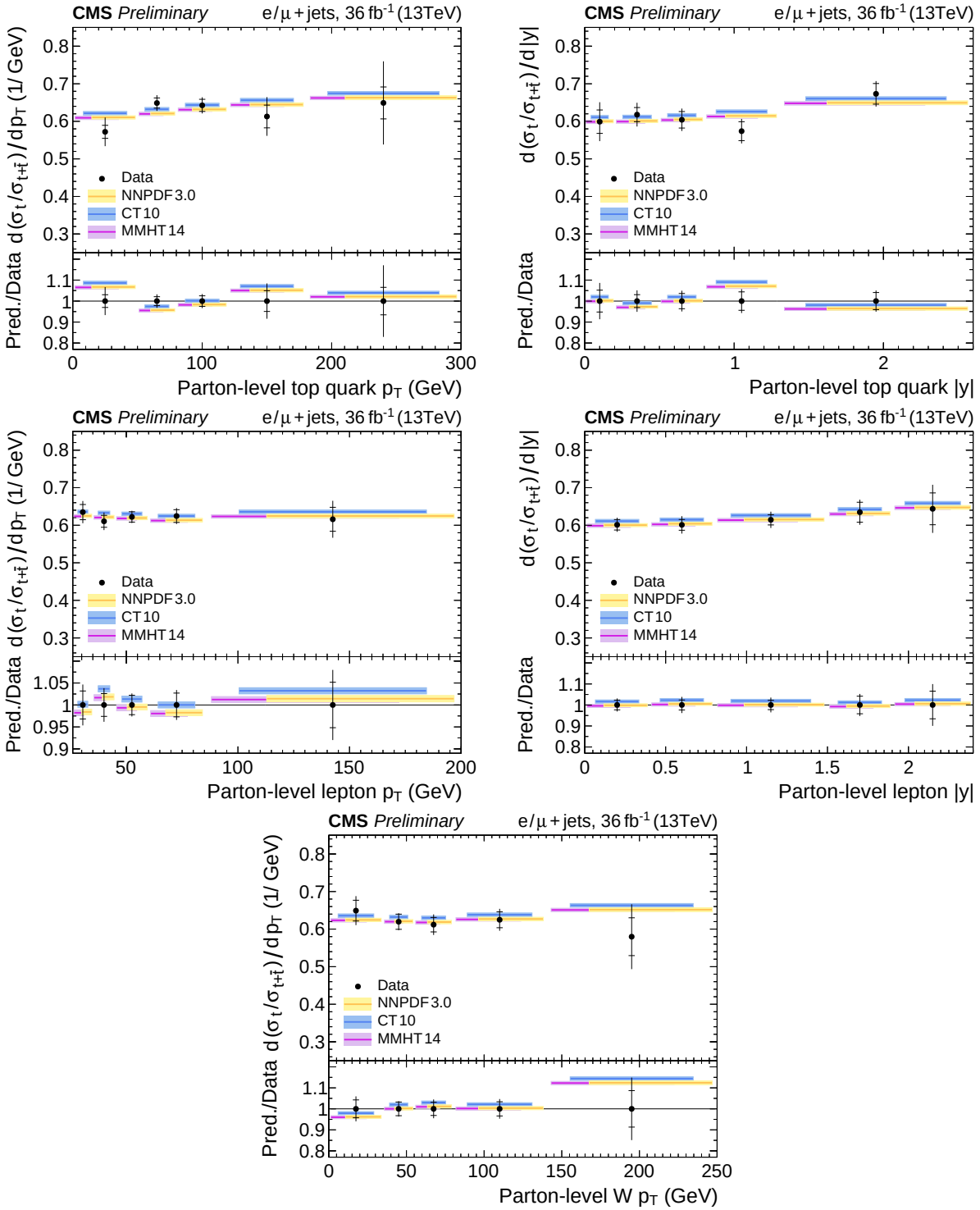

Figure 11: Differential t-channel single top quark charge ratios at parton level: (upper row) top quark p_{T} and rapidity; (middle row) charged lepton p_{T} and rapidity; (lower row) W boson p_{T}. The inner tick marks denote the unfolded post-fit uncertainty after the experimental systematic uncertainties have been profiled.

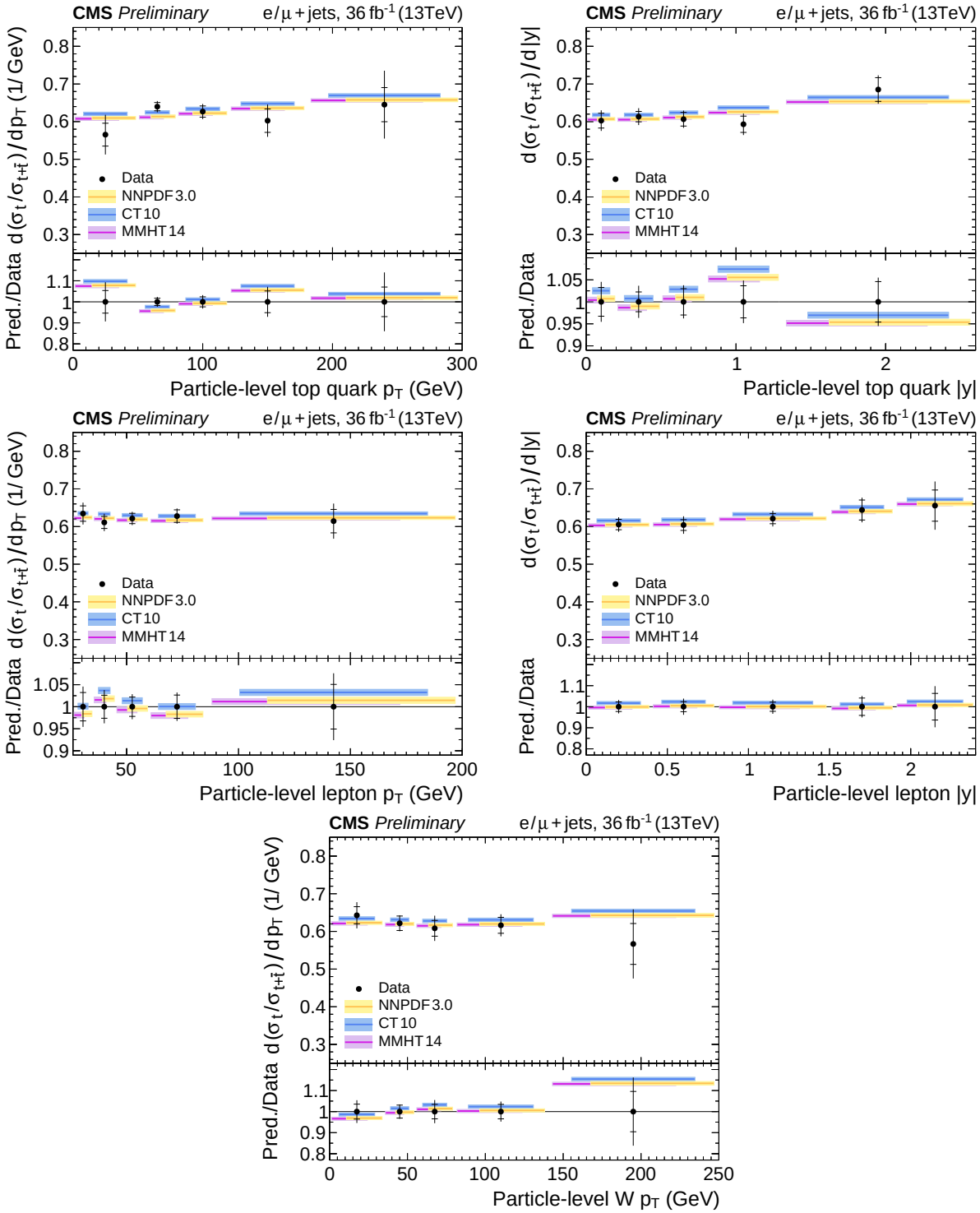

Figure 12: Differential t-channel single top quark charge ratios at particle level: (upper row) top quark p_{T} and rapidity; (middle row) charged lepton p_{T} and rapidity; (lower row) W boson p_{T}. The inner tick marks denote the unfolded post-fit uncertainty after the experimental systematic uncertainties have been profiled.

[3] M. Botje et al., "The PDF4LHC working group interim recommendations", arXiv:1101.0538.

[4] A. D. Martin, W. J. Stirling, R. S. Thorne, and G. Watt, "Parton distributions for the LHC", *Eur. Phys. J. C* **63** (2009) 189, doi:10.1140/epjc/s10052-009-1072-5, arXiv:0901.0002.

[5] A. D. Martin, W. J. Stirling, R. S. Thorne, and G. Watt, "Uncertainties on α_S in global PDF analyses and implications for predicted hadronic cross sections", *Eur. Phys. J. C* **64** (2009) 653, doi:10.1140/epjc/s10052-009-1164-2, arXiv:0905.3531.

[6] H.-L. Lai et al., "New parton distributions for collider physics", *Phys. Rev. D* **82** (2010) 074024, doi:10.1103/PhysRevD.82.074024, arXiv:1007.2241.

[7] R. D. Ball et al., "Parton distributions with LHC data", *Nucl. Phys. B* **867** (2013) 244, doi:10.1016/j.nuclphysb.2012.10.003, arXiv:1207.1303.

[8] E. L. Berger, J. Gao, C. P. Yuan, and H. X. Zhu, "NNLO QCD corrections to t-channel single top quark production and decay", *Phys. Rev. D* **94** (2016) 071501, doi:10.1103/PhysRevD.94.071501, arXiv:1606.08463.

[9] CDF Collaboration, "First observation of electroweak single top quark production", *Phys. Rev. Lett.* **103** (2009) 092002, doi:10.1103/PhysRevLett.103.092002, arXiv:0903.0885.

[10] D0 Collaboration, "Observation of single top quark production", *Phys. Rev. Lett.* **103** (2009) 092001, doi:10.1103/PhysRevLett.103.092001, arXiv:0903.0850.

[11] CMS Collaboration, "Measurement of the t-channel single top quark production cross section in pp collisions at $\sqrt{s} = 7$ *TeV*", *Phys. Rev. Lett.* **107** (2011) 091802, doi:10.1103/PhysRevLett.107.091802, arXiv:1106.3052.

[12] ATLAS Collaboration, "Comprehensive measurements of t-channel single top quark production cross sections at $\sqrt{s} = 7$ TeV with the ATLAS detector", *Phys. Rev. D* **90** (2014) 112006, doi:10.1103/PhysRevD.90.112006, arXiv:1406.7844.

[13] CMS Collaboration, "Measurement of the single top quark t-channel cross section in pp collisions at $\sqrt{s} = 7$ TeV", *JHEP* **12** (2012) 035, doi:10.1007/JHEP12(2012)035, arXiv:1209.4533.

[14] ATLAS Collaboration, "Fiducial, total and differential cross section measurements of t-channel single top quark production in pp collisions at 8 TeV using data collected by the ATLAS detector", *Eur. Phys. J. C* **77** (2017) 531, doi:10.1140/epjc/s10052-017-5061-9, arXiv:1702.02859.

[15] CMS Collaboration, "Cross section measurement of t-channel single top quark production in pp collisions at $\sqrt{s} = 13$ TeV", *Phys. Lett. B* **772** (2017) 752, doi:10.1016/j.physletb.2017.07.047, arXiv:1610.00678.

[16] ATLAS Collaboration, "Measurement of the inclusive cross sections of single top quark and top antiquark t-channel production in pp collisions at $\sqrt{s} = 13$ TeV with the ATLAS detector", *JHEP* **04** (2017) 086, doi:10.1007/JHEP04(2017)086, arXiv:1609.03920.

[17] CMS Collaboration, "Measurement of top quark polarisation in t-channel single top quark production", *JHEP* **04** (2016) 073, doi:10.1007/JHEP04(2016)073, arXiv:1511.02138.

[18] N. P. Hartland et al., "A Monte Carlo global analysis of the standard model effective field theory: the top quark sector", arXiv:1901.05965.

[19] S. Alekhin, J. Blümlein, S. Moch, and R. Placakyte, "Parton distribution functions, α_S, and heavy-quark masses for LHC Run II", *Phys. Rev. D* **96** (2017) 014011, doi:10.1103/PhysRevD.96.014011, arXiv:1701.05838.

[20] G. Mahlon and S. J. Parke, "Single top quark production at the LHC: Understanding spin", *Phys. Lett. B* **476** (2000) 323, doi:10.1016/S0370-2693(00)00149-0, arXiv:hep-ph/9912458.

[21] E. E. Boos and A. V. Sherstnev, "Spin effects in processes of single top quark production at hadron colliders", *Phys. Lett. B* **534** (2002) 97, doi:10.1016/S0370-2693(02)01659-3, arXiv:hep-ph/0201271.

[22] J. A. Aguilar-Saavedra and J. Bernabeu, "W polarisation beyond helicity fractions in top quark decays", *Nucl. Phys. B* **840** (2010) 349, doi:10.1016/j.nuclphysb.2010.07.012, arXiv:1005.5382.

[23] ATLAS Collaboration, "Probing the Wtb vertex structure in t-channel single-top-quark production and decay in pp collisions at $\sqrt{s} = 8$ TeV with the ATLAS detector", *JHEP* **04** (2017) 124, doi:10.1007/JHEP04(2017)124, arXiv:1702.08309.

[24] ATLAS Collaboration, "Analysis of the Wtb vertex from the measurement of triple-differential angular decay rates of single top quarks produced in the t-channel at $\sqrt{s} = 8$ TeV with the ATLAS detector", *JHEP* **12** (2017) 017, doi:10.1007/JHEP12(2017)017, arXiv:1707.05393.

[25] CMS Collaboration, "Object definitions for top quark analyses at the particle level", Technical Report CMS-NOTE-2017-004, 2017. https://cds.cern.ch/record/2267573.

[26] CMS Collaboration, "CMS luminosity measurements for the 2016 data taking period", Technical Report CMS-PAS-LUM-17-001, 2017. http://cds.cern.ch/record/2257069.

[27] CMS Collaboration, "Performance of electron reconstruction and selection with the CMS detector in proton-proton collisions at $\sqrt{s} = 8$ TeV", *JINST* **10** (2015) P06005, doi:10.1088/1748-0221/10/06/P06005, arXiv:1502.02701.

[28] S. Alioli, P. Nason, C. Oleari, and E. Re, "A general framework for implementing NLO calculations in shower Monte Carlo programs: the POWHEG BOX", *JHEP* **06** (2010) 043, doi:10.1007/JHEP06(2010)043, arXiv:1002.2581.

[29] R. Frederix, E. Re, and P. Torrielli, "Single top t-channel hadroproduction in the four-flavour scheme with POWHEG and aMC@NLO", *JHEP* **09** (2012) 130, doi:10.1007/JHEP09(2012)130, arXiv:1207.5391.

[30] T. Sjöstrand et al., "An Introduction to PYTHIA 8.2", *Comput. Phys. Commun.* **191** (2015) 159, doi:10.1016/j.cpc.2015.01.024, arXiv:1410.3012.

[31] CMS Collaboration, "Event generator tunes obtained from underlying event and multiparton scattering measurements", *Eur. Phys. J. C* **76** (2016) 155, doi:10.1140/epjc/s10052-016-3988-x, arXiv:1512.00815.

[32] P. Artoisenet, R. Frederix, O. Mattelaer, and R. Rietkerk, "Automatic spin-entangled decays of heavy resonances in Monte Carlo simulations", *JHEP* **03** (2013) 015, doi:10.1007/JHEP03(2013)015, arXiv:1212.3460.

[33] J. Alwall et al., "The automated computation of tree-level and next-to-leading order differential cross sections, and their matching to parton shower simulations", *JHEP* **07** (2014) 079, doi:10.1007/JHEP07(2014)079, arXiv:1405.0301.

[34] CMS Collaboration, "Investigations of the impact of the parton shower tuning in Pythia 8 in the modelling of $\mathrm{t\bar{t}}$ at $\sqrt{s} = 8$ and 13 TeV", Technical Report CMS-PAS-TOP-16-021, 2016. https://cds.cern.ch/record/2235192.

[35] E. Re, "Single top Wt-channel production matched with parton showers using the POWHEG method", *Eur. Phys. J. C* **71** (2011) 1547, doi:10.1140/epjc/s10052-011-1547-z, arXiv:1009.2450.

[36] S. Frixione et al., "Single top hadroproduction in association with a W boson", *JHEP* **07** (2008) 029, doi:10.1088/1126-6708/2008/07/029, arXiv:0805.3067.

[37] R. Frederix and S. Frixione, "Merging meets matching in MC@NLO", *JHEP* **12** (2012) 061, doi:10.1007/JHEP12(2012)061, arXiv:1209.6215.

[38] J. Alwall et al., "Comparative study of various algorithms for the merging of parton showers and matrix elements in hadronic collisions", *Eur. Phys. J. C* **53** (2008) 473, doi:10.1140/epjc/s10052-007-0490-5, arXiv:0706.2569.

[39] NNPDF Collaboration, "Parton distributions for the LHC Run II", *JHEP* **04** (2015) 040, doi:10.1007/JHEP04(2015)040, arXiv:1410.8849.

[40] GEANT4 Collaboration, "GEANT4 — a simulation toolkit", *Nucl. Instrum. Meth. A* **506** (2003) 250, doi:10.1016/S0168-9002(03)01368-8.

[41] CMS Collaboration, "Particle-flow reconstruction and global event description with the CMS detector", *JINST* **12** (2017) P10003, doi:10.1088/1748-0221/12/10/P10003, arXiv:1706.04965.

[42] CMS Collaboration, "The CMS experiment at the CERN LHC", *JINST* **3** (2008) S08004, doi:10.1088/1748-0221/3/08/S08004.

[43] M. Cacciari and G. P. Salam, "Pileup subtraction using jet areas", *Phys. Lett. B* **659** (2008) 119, doi:10.1016/j.physletb.2007.09.077, arXiv:0707.1378.

[44] M. Cacciari, G. P. Salam, and G. Soyez, "The anti-k_{T} jet clustering algorithm", *JHEP* **04** (2008) 063, doi:10.1088/1126-6708/2008/04/063, arXiv:0802.1189.

[45] M. Cacciari, G. P. Salam, and G. Soyez, "FastJet User Manual", *Eur. Phys. J. C* **72** (2012) 1896, doi:10.1140/epjc/s10052-012-1896-2, arXiv:1111.6097.

[46] CMS Collaboration, "Pileup removal algorithms", Technical Report CMS-PAS-JME-14-001, 2014. https://cds.cern.ch/record/1751454.

[47] CMS Collaboration, "Identification of heavy-flavour jets with the CMS detector in pp collisions at 13 TeV", *JINST* **13** (2018) P05011, doi:10.1088/1748-0221/13/05/P05011, arXiv:1712.07158.

[48] CMS Collaboration, "Performance of CMS muon reconstruction in pp collision events at $\sqrt{s} = 7$ TeV", *JINST* **7** (2012) P10002, doi:10.1088/1748-0221/7/10/P10002, arXiv:1206.4071.

[49] S. Kallweit et al., "NLO QCD+EW predictions for V+jets including off-shell vector-boson decays and multijet merging", *JHEP* **04** (2016) 021, doi:10.1007/JHEP04(2016)021, arXiv:1511.08692.

[50] F. R. Anger, F. Febres Cordero, H. Ita, and V. Sotnikov, "NLO QCD predictions for $\mathrm{Wb\bar{b}}$ production in association with up to three light jets at the LHC", *Phys. Rev. D* **97** (2018) 036018, doi:10.1103/PhysRevD.97.036018, arXiv:1712.05721.

[51] R. Barlow and C. Beeston, "Fitting using finite Monte Carlo samples", *Comput. Phys. Commun.* **77** (1993) 219, doi:https://doi.org/10.1016/0010-4655(93)90005-W.

[52] S. Schmitt, "TUnfold: An algorithm for correcting migration effects in high energy physics", *JINST* **7** (2012) T10003, doi:10.1088/1748-0221/7/10/T10003, arXiv:1205.6201.

[53] A. Tikhonov, "Solution of incorrectly formulated problems and the regularization method", *Soviet Math. Dokl.* **5** (1963) 1035.

[54] V. Blobel, "An unfolding method for high energy physics experiments", in *Advanced statistical techniques in particle physics, Proceedings, Conference, Durham, UK, March 18–22, 2002*, pp. 258–267. 2002. arXiv:hep-ex/0208022.

[55] CMS Collaboration, "Determination of jet energy calibration and transverse momentum resolution in CMS", *JINST* **6** (2011) P11002, doi:10.1088/1748-0221/6/11/P11002, arXiv:1107.4277.

[56] CMS Collaboration, "Performance of the CMS missing transverse momentum reconstruction in pp data at $\sqrt{s} = 8$ TeV", *JINST* **10** (2015) P02006, doi:10.1088/1748-0221/10/02/P02006, arXiv:1411.0511.

[57] CMS Collaboration, "Measurement of the inelastic proton-proton cross section at $\sqrt{s} = 13$ TeV", *JHEP* **07** (2018) 161, doi:10.1007/JHEP07(2018)161, arXiv:1802.02613.

[58] CMS Collaboration, "Performance of the CMS muon detector and muon reconstruction with proton-proton collisions at $\sqrt{s} = 13$ TeV", *JINST* **13** (2018) P06015, doi:10.1088/1748-0221/13/06/P06015, arXiv:1804.04528.

[59] CMS Collaboration, "Measurement of the differential cross section for top quark pair production in pp collisions at $\sqrt{s} = 8$ TeV", *Eur. Phys. J. C* **75** (2015) 542, doi:10.1140/epjc/s10052-015-3709-x, arXiv:1505.04480.

[60] CMS Collaboration, "Measurement of differential cross sections for top quark pair production using the lepton+jets final state in proton-proton collisions at 13 TeV", *Phys. Rev. D* **95** (2017) 092001, doi:10.1103/PhysRevD.95.092001, arXiv:1610.04191.

[61] A. Kalogeropoulos and J. Alwall, "The SysCalc code: A tool to derive theoretical systematic uncertainties", arXiv:1801.08401.

[62] L. A. Harland-Lang, A. D. Martin, P. Motylinski, and R. S. Thorne, "Parton distributions in the LHC era: MMHT 2014 PDFs", *Eur. Phys. J. C* **75** (2015) 204, doi:10.1140/epjc/s10052-015-3397-6, arXiv:1412.3989.